Calculations of two-neutrino double-β decay for fpg shell nuclei

Hantao Li (李瀚涛)[1,*] and Zhongzhou Ren (任中洲)[2,†]
[1]*School of Science, North University of China, Taiyuan 030051, China*
[2]*School of Physics Science and Engineering, Tongji University, Shanghai 200092, China*
(Received 23 July 2017; revised manuscript received 7 November 2017; published 28 December 2017)

In this paper, we calculate the properties of two-neutrino double-β ($2\nu\beta\beta$) decays for nuclei within fpg ($1p_{3/2}, 0f_{5/2}, 1p_{1/2}, 0g_{9/2}$) shell model space systematically under the framework of the nuclear shell model. Both of the decays on the β^- side ($2\nu 2\beta^-$) and the mixed β^+ and electron capture types ($2\nu 2\beta^+$, $2\nu\beta^+$EC, and 2νECEC) are taken into consideration. Results of the calculated half lives, nuclear matrix elements (NMEs), phase space factors, and branching ratios are shown. Good agreements between theory and experiments have been reached. Accumulations of the NMEs are also analyzed which do not support the single-state dominance hypothesis. The half lives of the nuclei ^{86}Kr, ^{70}Zn, and ^{84}Sr are predicted to be 4.2×10^{22}, 1.4×10^{23}, and 1.9×10^{23} years respectively which appears attractive for future experimental probing.

DOI: 10.1103/PhysRevC.96.065503

I. INTRODUCTION

The two-neutrino double-β decay is a second order weak-interaction process which was discussed by Mayer [1] in 1935. After that it took more than 50 years for this process to be observed directly in the laboratory [2]. So far the $2\nu\beta\beta$ decay is with the longest lifetime for all the radioactive processes ever observed [3–8]. Detection of the $2\nu\beta\beta$ decay renews the knowledge of unstable nuclei, i.e., some isotopes which were earlier considered to be stable are not. The $2\nu\beta\beta$ decay is also considered to be important by theorists [9]. Half lives of the $2\nu\beta\beta$ decay depend on the inverse of the squared nuclear matrix elements (NMEs) which relay on the nuclear structures. Many nuclear models have been used to describe the wave functions of the associated nuclei, such as the quasiparticle random-phase approximation (QRPA) [10–14], the nuclear shell model [11,15–17], and the interacting boson model [18].

The $2\nu\beta\beta$ decays can be classified into two categories: The $2\nu 2\beta^-$ decays, which have favored Q values and abundances [19], have been extensively researched from both of the experimental and theoretical aspects [3,20,21]. Many decays of the $2\nu 2\beta^-$ type have been detected which include transitions to the ground and excited states [22,23]. Another category of the $2\nu\beta\beta$ is the mixed β^+ and electron capture decays ($2\nu 2\beta^+$, $2\nu\beta^+$EC, and 2νECEC, generally called $2\nu\beta^+$/EC hereafter) which are much less studied. For a long period of time the $2\nu\beta^+$/EC decays are considered to be just out of research. However, in very recent years interest in the $2\nu\beta^+$/EC decays has been renewed [24–26]. The half life of the 2ν2K capture for the ^{78}Kr nuclei has been observed by recent experiment [27] and many theoretical researches for the $2\nu\beta^+$/EC decays have been carried out [19,28–31].

Precise knowledge of the NMEs plays an important role in the evaluations of the half lives for the $2\nu\beta\beta$ decay. However, the associated NMEs are notoriously difficult to calculate [32,33]. Theoretically there exists the single-state dominance hypothesis (SSDH) [34–37] which suggests that the NMEs for $2\nu\beta\beta$ are solely determined by virtual single-β transitions via the 1^+ ground state of the intermediate nucleus. If the SSDH is confirmed, the corresponding NME could be determined from β decay measurements which are much easier to be carried out [35]. Thus, it is of great importance to check the validity of the SSDH.

The mass region for the observed $2\nu\beta\beta$ nuclei is rather large. Shell model calculations can be used to obtain the wave functions for nuclei in the light and medium mass regions. Within these mass regions, the fpg shell nuclei are of interest. In total, nine double-β emitters, including ^{78}Kr whose 2ν2K capture was observed recently, belong to this shell. The fpg shell nuclei are of interest for the structure variation around the semimagic shell closure at $N = 40$. Another interesting feature for these nuclei is the shape evolution in the $A = 70$ region. For the $2\nu\beta\beta$ nuclei concerned in this paper, the nuclei ^{70}Zn and ^{74}Se are with neutron number $N = 40$. In addition the nuclei ^{74}Se, ^{76}Ge, ^{78}Kr, and ^{80}Se are open-shell nuclei and most of the corresponding calculations are performed within the pnQRPA approach and its extensions [16]. Thus, it is of interest to carry out shell model calculations for the double-β decays for nuclei within the fpg shell.

In this paper, the $2\nu 2\beta^-$ and $2\nu\beta^+$/EC decays for the fpg shell nuclei are studied systematically under the framework of nuclear shell model. Transitions to the excited states are also taken into consideration. Calculated results for the half lives, NMEs, phase space factors, and branching ratios are shown. The calculated half lives agree well with the existing experimental data. Also, half lives of the $2\nu\beta\beta$ decays for six nuclei are predicted. We analyzed the accumulations of the NMEs and find that the viewpoint of the SSDH is violated.

II. OUTLINE OF THE THEORETICAL FRAMEWORK

A. Formulas of the $2\nu\beta\beta$ decays

Half lives of the $2\nu\beta\beta$ decays are determined by the phase factors ($G_{2\nu}$) and the NMEs ($M_{2\nu}$) [9],

$$\left[t_{1/2}^{2\nu}\right]^{-1} = G_{2\nu}|M_{2\nu}|^2. \quad (1)$$

*lihantao@nuc.edu.cn
†zren@tongji.edu.cn; zren@nju.edu.cn

Four types of the $2\nu\beta\beta$ decays are considered to exist ($2\nu 2\beta^-$, $2\nu 2\beta^+$, $2\nu\beta^+$EC, and 2νECEC). Expressions for the phase space factors are different for each type. Formulas for the phase space factors can be found in Ref. [9] for the $2\nu 2\beta^-$ decay and in Refs. [9,28,38] for the $2\nu\beta^+$/EC decays. The phase space factors for the $2\nu\beta\beta$ decays depend on the fourth power of the axial-vector coupling constant g_A. Hence it is of importance to adopt a reliable value for the g_A. In this work, a commonly used value of $g_A = 1.27$ [39,40] is adopted.

The NMEs for the $2\nu\beta\beta$ decays have dependence on the decay mode and the angular momentum of the final state [28],

$$M^{\alpha}_{2\nu}(J^+) = \sum_m M_m(J^+) F^{\alpha}_m(J^+). \tag{2}$$

Here the sum is over all the involved intermediate 1^+_m states, the superscript α denotes for the type of the decay, J^+ is the angular momentum and parity for the final state. In the framework of the nuclear shell model the $M_m(J^+)$ in Eq. (2) has the form of [9,28,41]

$$M_m(J^+) = \frac{\langle J^+_f \| \sum_a \sigma_a \tau^{\pm}_a \| 1^+_m \rangle \langle 1^+_m \| \sum_b \sigma_b \tau^{\pm}_b \| 0^+_{g.s.} \rangle}{\sqrt{1 + 2\delta_{J2}}}, \tag{3}$$

with τ^- (τ^+) corresponding to the $2\nu 2\beta^-$($2\nu\beta^+$/EC) decays, the sums are for all possible nucleons, and δ is the Dirac delta function. The matrix elements are reduced with respect to the angular momentum. The $|0^+_{g.s.}\rangle$ and $\langle J^+_f|$ denote the initial and final nuclear states, respectively. The quantities $F^{\alpha}_m(J^+)$ in Eq. (2) are the energy denominators which can be cast in the form [28]

$$F^{2\beta^-}_m(0^+) = F^{2\beta^+}_m(0^+) = \left(\Delta_m + \tfrac{1}{2}W_0\right)^{-1}, \tag{4}$$

$$F^{2\beta^-}_m(2^+) = F^{2\beta^+}_m(2^+) = \left(\Delta_m + \tfrac{1}{2}W_0\right)^{-3}, \tag{5}$$

$$F^{\beta^+\mathrm{EC}}_m(0^+) = \left(\Delta_m - \varepsilon_{b1} + \tfrac{1}{3}W_0^{\beta^+\mathrm{EC}}\right)^{-1} + \left(\Delta_m + \tfrac{2}{3}W_0^{\beta^+\mathrm{EC}}\right)^{-1}, \tag{6}$$

$$F^{\beta^+\mathrm{EC}}_m(2^+) = \left(\Delta_m + \tfrac{1}{2}W_0\right)\left(\Delta_m - \varepsilon_{b1} + \tfrac{1}{3}W_0^{\beta^+\mathrm{EC}}\right)^{-2} \times \left(\Delta_m + \tfrac{2}{3}W_0^{\beta^+\mathrm{EC}}\right)^{-2}, \tag{7}$$

$$F^{\mathrm{ECEC}}_m(0^+) = \left(\Delta_m - \varepsilon_{b1} + \tfrac{1}{2}W_0^{\mathrm{ECEC}}\right)^{-1} + \left(\Delta_m - \varepsilon_{b2} + \tfrac{1}{2}W_0^{\mathrm{ECEC}}\right)^{-1}, \tag{8}$$

$$F^{\mathrm{ECEC}}_m(2^+) = \left(\Delta_m + \tfrac{1}{2}W_0\right)\left(\Delta_m - \varepsilon_{b1} + \tfrac{1}{2}W_0^{\mathrm{ECEC}}\right)^{-2} \times \left(\Delta_m - \varepsilon_{b2} + \tfrac{1}{2}W_0^{\mathrm{ECEC}}\right)^{-2}, \tag{9}$$

where

$$\begin{aligned} \Delta_m &= (E_m - M_i c^2)/(m_e c^2), \\ W_0 &= (M_i c^2 - E_f)/(m_e c^2), \\ W_0^{\beta^+\mathrm{EC}} &= W_0 + \varepsilon_{b1}, \\ W_0^{\mathrm{ECEC}} &= W_0 + \varepsilon_{b1} + \varepsilon_{b2}. \end{aligned} \tag{10}$$

Here E_m and E_f denote the energies of intermediate and final nuclear states, respectively. The quantity M_i is the mass for initial nucleus, and m_e is the mass of electron, $\varepsilon_b = (m_e c^2 - B_i)/m_e c^2$ is the total energy for captured electron with B_i the binding energy of the captured electron [28]. All the values of M_i, E_m, and E_f are for the nucleus which are hard to measure and usually one has to use the atomic masses. A relation between the nuclear mass M and atomic mass $\mathcal{M}(A,Z)$ is discussed in Ref. [38],

$$\mathcal{M}(A,Z) = M + Z m_e - B(Z). \tag{11}$$

Here $B(Z)$ stands for the total electron binding energy whose evaluation is a complicated problem. In the numerical calculations throughout this paper, $B(Z-2) = B(Z-1) = B(Z)$ is assumed [38].

B. Discussions of the shell model calculations

Our calculations are carried out in the fpg shell model space without any truncation and the JUN45 effective interaction [42] is adopted. This effective interaction is derived from a realistic interaction based on the Bonn-C potential and 133 two-body matrix elements and four single-particle energies are modified empirically so as to fit the experimental energy data [42]. This effective interaction has been tested to study the Ge isotopes around $N = 40$, the $N = Z$ nuclei with $A = 64$–70, and the $N = 49$ odd-odd nuclei which turns out to describe rather well the properties related to the $g_{9/2}$ orbit in various cases [42]. As the nuclei concerned in this paper are not far from these regions, it is reasonable to adopt the JUN45 effective interaction for the corresponding calculations.

The computer program NUSHELLX [43] is used to calculate the wave functions for the involved nuclear states. 50 intermediate 1^+ states are considered in the calculations of the $M_{2\nu}$ for all the involved nucleus.

In shell model calculations a quenching factor is needed as a correction for the transition strength. One reliable method for evaluating this factor is comparing the $T(GT)$ values which are defined by Ref. [44]. We calculate the Gamow-Teller strengths for β decay of 16 nuclei in this region (^{64}Cu, $^{63-65}$Ga, ^{68}Ga, ^{70}Ga, $^{64-68}$Ge, ^{67,68}As, ^{68}Se, and ^{78}Br) and compare them with the experimental data [45–53]. Note that most of these nuclei can decay by Gamow-Teller and forbidden transitions. The forbidden transitions are complex where various transition matrix elements and quenching factors are involved in [54,55]. In calculations of the NMEs of the $2\nu\beta\beta$ decay in Eq. (3), only the $\sigma \cdot \tau$ operator is involved which does not appead6r in the matrix elements for forbidden transitions. Thus, data of forbidden transitions are not adopted to evaluate the quenching factor in this paper.

The experimental $T(GT)$ values are given as follows: The nucleus ^{68}Ge decays solely to the ground state of ^{68}Ga. The $\log_{10} ft$ value for this transition is measured to be 5.01 [50]. Using Eqs. (3)–(7) in Ref. [44], the experimental $B(GT)$, $M(GT)$, $R(GT)$, and $T(GT)$ values are calculated to be 0.0606, 0.246, 0.0559, and 0.0559, respectively. The nucleus ^{68}Se can decay to the 1^+_1 and 1^+_2 states of ^{68}As. The $\log_{10} ft$ values for these two transitions are measured to be 4.15 and

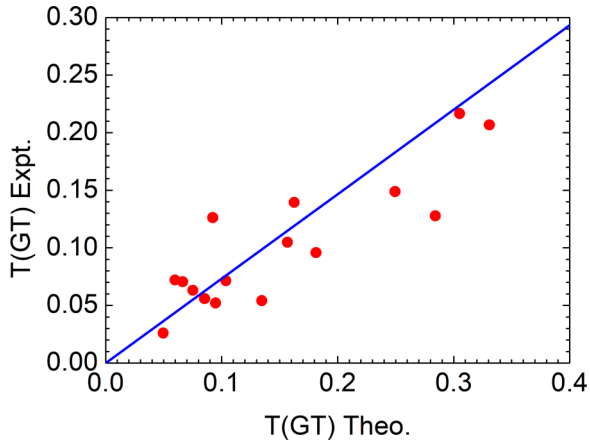

FIG. 1. Comparison of the calculated $T(GT)$ values with the experimental data. Each point represent a nucleus where the vertical and horizontal axis are the associated experimental and calculated $T(GT)$ values, respectively.

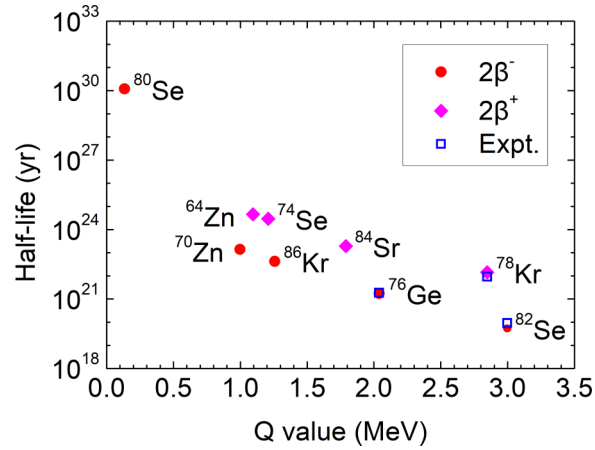

FIG. 2. Half lives for the $2\nu\beta\beta$ decays of the fpg shell nuclei. The vertical axis is for the half lives in $\log_{10}$ frame in the units of yr while the horizontal axis for the Q values is in units of MeV. Decays for the $2\nu 2\beta^-$ and $2\nu\beta^+$/EC types are represented by triangles and diamonds, respectively. Hollow squares are for the experimental data.

5.43 [50], respectively. Using Eqs. (3)–(6) in Ref. [44], one obtains the $R(GT)$ values of these two transitions 0.123 and 0.0280. The $T(GT)$ value is a summing of the total strength. Using Eq. (7) in Ref. [44], one gets $T(GT) = 0.126$ for the decay of ^{68}Se.

The results for calculated and experimental $T(GT)$ values are shown in Fig. 1. In Fig. 1 each point represents a nucleus where the vertical and horizontal axes are the associated experimental and calculated $T(GT)$ values, respectively. The points follow a straight line whose slope is the averaged quenching factors $q = 0.73 \pm 0.07$. This value is consistent with the quenching factor $q = 0.74$ for pf shell [39,44] and $q = 0.71$ for $sdpf$ shell [39]. In Ref. [15], no quenching factor is included and $g_A = 1$–1.261 is used. In Ref. [56], $g_A = 1$ is adopted to take into account the reduction of the Gamow-Teller strength which yields the same result as $g_A = 1.27$ with $q = 0.79$. Thus, the value $q = 0.73 \pm 0.07$ is adopted for all the calculations in this work.

III. RESULTS AND DISCUSSIONS

One interesting feature of the $2\nu\beta\beta$ decay is its extremely long half life. In Table I the calculated half lives of the $2\nu\beta\beta$ decays for the fpg shell nuclei are compared with the experimental data. Column 1 is for the concerned nuclei. Column 2 lists the types of the $2\nu\beta\beta$ decays where $2\beta^-$ and $2\beta^+$ denote for the $2\nu 2\beta^-$ and $2\nu\beta^+$/EC, respectively. The Q values adopted in the calculations, which are from the recent atomic mass evaluation [58], are in column 3. Column 4 shows the calculated half lives where errors in the parentheses originate from the error of the quenching factor. Experimental half lives are listed in columns 5 and 6. It should be noted that for the ^{78}Kr nucleus, the experimental half life is for the 2ν2K capture. It can be seen from Table I that agreements between theory and experiments are good.

Half lives of the $2\nu\beta\beta$ decays are largely affected by Q values. In Fig. 2 the half lives are plotted as a function

TABLE I. Comparison between the calculated half lives and the recent experiments. Column 1 is for the concerned nuclei. Column 2 lists the types of the $2\nu\beta\beta$ decays where $2\beta^-$ and $2\beta^+$ denote for the $2\nu 2\beta^-$ and $2\nu\beta^+$/EC, respectively. The Q values adopted in the calculations are listed in column 3. Columns 4–6 are for the calculated and experimental half lives, respectively. The error given in the parentheses for the calculated half lives originates from the error of the quenching factor. Half lives are in units of year while the Q values are in units of keV. Note that the experimental values of the ^{78}Kr are for the 2ν2K capture.

Nucleus	Type	Q value	Half life (yr)		
		(keV)	Theor.	Expt.	
^{64}Zn	$2\beta^+$	1094.9	$4.6(18) \times 10^{24}$	$\geqslant 1.1 \times 10^{19}$ [57]	
^{70}Zn	$2\beta^-$	997.1	$1.4(5) \times 10^{23}$	$\geqslant 3.8 \times 10^{18}$ [57]	
^{74}Se	$2\beta^+$	1209.24	$2.9(11) \times 10^{24}$	$> 1.5 \times 10^{19}$ [58]	
^{76}Ge	$2\beta^-$	2039.06	$1.8(7) \times 10^{21}$	$(1.84^{+0.14}_{-0.10}) \times 10^{21}$ [59]	$(1.66 \pm 0.13) \times 10^{21}$ [58]
^{78}Kr	$2\beta^+$	2847.67	$14(5) \times 10^{21}$	$(9.2^{+5.5}_{-2.6} \pm 1.3) \times 10^{21}$ [27]	
^{80}Se	$2\beta^-$	133.9	$1.2(5) \times 10^{30}$		
^{82}Se	$2\beta^-$	2997.9	$5.3(21) \times 10^{19}$	$(9.1 \pm 0.3 \pm 1.0) \times 10^{19}$ [4]	$(9.2 \pm 0.7) \times 10^{19}$ [58]
^{84}Sr	$2\beta^+$	1789.8	$1.9(7) \times 10^{23}$		
^{86}Kr	$2\beta^-$	1257.42	$4.2(16) \times 10^{22}$		

TABLE II. Details of the $2\nu2\beta^-$ decays for the fpg shell nuclei. Column 1 is for the concerned nuclei. Excitation energies and J^π for final states are listed in columns 2 and 3, respectively. Absolute values of the calculated NMEs are in column 4 and results from other works are listed in column 5 for comparison. Column 6 is for the phase space factors and column 7 is for the branching ratios of each transition. The last two columns are calculated and experimental half lives, respectively. The error given in the parentheses for the calculated NMEs and half lives originates from the error of the quenching factor.

Nucleus	J_f^π	Ex.	$\lvert M_{GT}^{2\nu}\rvert$		$G_{2\nu}$ (yr^{-1})	Br.	$t_{1/2}^{2\nu}$ (yr)	
		(keV)	This work	Others			Theor.	Expt.
^{70}Zn	$0^+_{g.s.}$	0	0.15(6)	0.447 [10]	3.243×10^{-22}	1.000	$1.4(5) \times 10^{23}$	$\geqslant 3.8 \times 10^{18}$ [57]
^{76}Ge	$0^+_{g.s.}$	0	0.064(25)	$0.0655^{+0.0019}_{-0.0024}$ [3]	1.382×10^{-19}	0.9990	$1.8(7) \times 10^{21}$	$(1.84^{+0.14}_{-0.10}) \times 10^{21}$ [59]
				0.074 [12]				
	0^+_1	1122	0.053(20)	0.130 [12]	2.006×10^{-22}	9.983×10^{-3}	$1.8(7) \times 10^{24}$	$>3.7 \times 10^{23}$ [23]
	2^+_1	559	0.00058(22)	0.0006 [13]	1.228×10^{-21}	7.243×10^{-7}	$2.4(9) \times 10^{27}$	$>1.6 \times 10^{23}$ [23]
				0.003 [12]				
	2^+_2	1216	0.00060(23)	0.012 [12]	1.043×10^{-24}	6.469×10^{-10}	$2.7(10) \times 10^{30}$	$>2.3 \times 10^{23}$ [23]
^{80}Se	$0^+_{g.s.}$	0	0.073(28)		1.592×10^{-28}	1.000	$1.2(5) \times 10^{30}$	
^{82}Se	$0^+_{g.s.}$	0	0.063(24)	$0.0509^{+0.0021}_{-0.0018}$ [3]	4.653×10^{-18}	0.9999	$5.3(21) \times 10^{19}$	$(9.1 \pm 0.3 \pm 1.0) \times 10^{19}$ [4]
				0.046 [12]				
	0^+_1	1488	0.010(4)	0.228 [12]	1.321×10^{-20}	7.746×10^{-5}	$6.9(26) \times 10^{23}$	$>3.4 \times 10^{22}$ [60]
	2^+_1	777	0.00064(24)	0.0002 [13]	2.228×10^{-19}	4.840×10^{-6}	$1.1(4) \times 10^{25}$	$>1.3 \times 10^{22}$ [60]
				0.0018 [12]				
				0.00012 [14]				
	2^+_2	1475	0.0015(6)	0.061 [12]	2.071×10^{-21}	2.358×10^{-7}	$2.3(9) \times 10^{26}$	$>1.0 \times 10^{22}$ [60]
				0.0094 [14]				
^{86}Kr	$0^+_{g.s.}$	0	0.082(31)	0.110 [10]	3.353×10^{-21}	1.000	$4.2(16) \times 10^{22}$	

of the Q value in $\log_{10}$ frame. Calculated half lives of the $2\nu2\beta^-$ and $2\nu\beta^+$/EC are represented by triangles and diamonds, respectively. Experimental data are represented by hollow squares. All the data involved are from Table I. Good agreements between theory and experiment are reached and we also predict the half lives for six nuclei. Due to the small Q value, the half life of ^{80}Se is predicted much longer than other concerned nuclei ($t_{1/2} = 1.2 \times 10^{30}$ yr), which is hard to measure by recent experiments.

It is obvious from Fig. 2 that with similar Q values, half lives for $2\nu\beta^+$/EC are systematically longer than that of $2\nu2\beta^-$ decays. In the $2\nu\beta^+$/EC decay, the 2νECEC process is dominant. When Q values are equal, a phase factor of the 2νECEC is obviously smaller than that of the $2\nu2\beta^-$ decay which leads to a longer half life for the $2\nu\beta^+$/EC.

Calculated results show that besides the nuclei ^{76}Ge, ^{82}Se, and ^{78}Kr whose half lives have been measured, ^{86}Kr is predicted to have the shortest half life ($t_{1/2} = 4.2 \times 10^{22}$ years) which may be detected by the recent experiments. The nuclei ^{70}Zn and ^{84}Sr are also predicted to have relatively short half lives of 1.4×10^{23} and 1.9×10^{23} yr, respectively.

Under the framework of the nuclear shell model, transitions to both the ground and excited states can be calculated. Details about the $2\nu2\beta^-$ decays for the fpg shell nuclei are listed in Table II where the first column is for the concerned nuclei. The J^π and the excitation energies for final states are listed in columns 2 and 3, respectively. Absolute values of the calculated NMEs are in column 4 and results from other works are listed in column 5 for comparison. Column 6 is for the phase space factors and column 7 is for the branching ratios of each transition. The last two columns are calculated and experimental half lives, respectively.

The NMEs listed in column 5 are from either the QRPA approach [10,12–14] or evaluated from experimental data [3]. The calculated results keep in line with the results from [3,10,13,14]. For transitions to the excited states, the calculated NMEs are systematically smaller than the data from Ref. [12] which are given by the renormalized pnQRPA approach. As the associated experimental data are not available, it is hard to judge which is better.

The NMEs for decays to the 2^+ state are significantly smaller than those of the decays to ground state as illustrated in Table II. This result agrees with the viewpoint of Refs. [14,28]. Due to the relatively smaller NMEs, transitions to the 2^+ states are difficult to observe.

Details of the $2\nu\beta^+$/EC decays for the fpg shell nuclei are presented in Table III. Column 1 is for the concerned nuclei. The J^π and the excitation energies for final states are listed in columns 2 and 3, respectively. Column 4 is for the types of the transitions. Column 5 is for the absolute value for the calculated NMEs ($M_{2\nu}^{2\beta^+}$, $M_{2\nu}^{\beta^+\mathrm{EC(K)}}$, and $M_{2\nu}^{\mathrm{EC(K)EC(K)}}$). As can be seen from Eqs. (6)–(10), differences between the NMEs for the K and L shell electron captures are very small. Thus, NMEs for the L capture are not listed. Column 6 lists the NMEs from others. Values for the $G_{2\nu}$ are listed in column 7. For all transitions the 2νECEC type has the largest phase space factor because the energy released by this transition is the largest. Column 8 is the branching ratios for each transition. Columns 9 and 10 are the calculated and experimental half lives, respectively.

TABLE III. Details of the $2\nu\beta^+$/EC decays for the fpg shell nuclei. Column 1 is for the concerned nuclei. The J^π and the excitation energies for final states are listed in columns 2 and 3, respectively. Column 4 is for the type of the transition. Column 5 is for the absolute value for the calculated NMEs ($M_{2\nu}^{2\beta^+}$, $M_{2\nu}^{\beta^+\mathrm{EC(K)}}$, and $M_{2\nu}^{\mathrm{EC(K)EC(K)}}$). Column 6 lists the NMEs from others. Values for the $G_{2\nu}$ are listed in column 7. Column 8 is the branching ratios for each transition. Columns 9 and 10 are the calculated and experimental half-lives, respectively. The error given in the parentheses for the calculated NMEs and half-lives originate from error of the quenching factor.

Nucleus	J_f^π	Ex.	Process	$\lvert M_{GT}^{2\nu}\rvert$		$G_{2\nu}$ (yr^{-1})	Br.	$t_{1/2}^{2\nu}$ (yr)	
		(keV)		This work	Others			Theor.	Expt.
^{64}Zn	$0_{g.s.}^+$	0	β^+EC	0.24(9)		1.039×10^{-32}	2.836×10^{-9}	$1.6(6) \times 10^{33}$	$\geqslant 9.4 \times 10^{20}$ [57]
			ECEC	0.23(9)		4.007×10^{-24}	1.000	$4.6(18) \times 10^{24}$	$\geqslant 1.1 \times 10^{19}$ [57]
^{74}Se	$0_{g.s.}^+$	0	β^+EC	0.15(6)	0.0359 [15]	2.952×10^{-29}	1.918×10^{-6}	$1.5(6) \times 10^{30}$	
			ECEC	0.15(6)	0.0446 [15]	1.591×10^{-23}	1.000	$2.9(11) \times 10^{24}$	
	2_1^+	596	ECEC	0.00038(14)	0.00288 [15]	1.090×10^{-25}	4.510×10^{-8}	$6.4(25) \times 10^{31}$	$>9.2 \times 10^{18}$ [61]
^{78}Kr	$0_{g.s.}^+$	0	$2\beta^+$	0.076(29)	0.247 [12]	2.627×10^{-25}	2.163×10^{-5}	$6.6(25) \times 10^{26}$	$\geqslant 2.0 \times 10^{21}$ [62]
			β^+EC	0.16(6)	0.37 [14]	1.050×10^{-21}	0.3881	$3.7(14) \times 10^{22}$	$\geqslant 1.1 \times 10^{20}$ [62]
			ECEC	0.15(6)		1.848×10^{-21}	0.6086	$24(9) \times 10^{21}$	$(9.2^{+5.5}_{-2.6}) \times 10^{21}$ [27]
	0_1^+	1499	β^+EC	0.077(30)	0.067 [12]	2.631×10^{-27}	2.259×10^{-7}	$6.4(24) \times 10^{28}$	
			ECEC	0.074(28)	0.076 [14]	4.183×10^{-23}	3.296×10^{-3}	$4.4(17) \times 10^{24}$	$\geqslant 5.4 \times 10^{21}$ [27]
	0_2^+	1759	β^+EC	0.0064(25)		3.158×10^{-33}	1.871×10^{-15}	$7.7(29) \times 10^{36}$	
			ECEC	0.0057(22)		1.400×10^{-23}	6.607×10^{-6}	$2.2(8) \times 10^{27}$	
	2_1^+	614	$2\beta^+$	0.00069(26)	0.00078 [12]	1.260×10^{-31}	8.515×10^{-16}	$1.7(6) \times 10^{37}$	
			β^+EC	0.00081(31)	0.0018 [14]	5.095×10^{-23}	4.853×10^{-7}	$3.0(11) \times 10^{28}$	
			ECEC	0.00069(26)		1.163×10^{-22}	7.858×10^{-7}	$1.8(7) \times 10^{28}$	
	2_2^+	1309	β^+EC	0.000042(16)	0.00081 [12]	8.873×10^{-26}	2.241×10^{-12}	$6.4(25) \times 10^{33}$	
			ECEC	0.0000041(16)	0.0017 [14]	1.774×10^{-23}	4.210×10^{-12}	$3.4(13) \times 10^{33}$	
	2_3^+	1996	ECEC	0.0016(6)		8.829×10^{-25}	3.258×10^{-8}	$4.4(17) \times 10^{29}$	
^{84}Sr	$0_{g.s.}^+$	0	β^+EC	0.14(5)	0.0744 [17]	1.987×10^{-24}	7.883×10^{-3}	$2.5(9) \times 10^{25}$	
			ECEC	0.14(5)	0.0742 [17]	2.623×10^{-22}	0.9921	$2.0(7) \times 10^{23}$	
	2_1^+	882	ECEC	0.00081(31)		1.823×10^{-24}	2.340×10^{-7}	$8.3(32) \times 10^{29}$	

The NMEs shown in column 6 are from the deformed shell model [15,17] and the QRPA [12,14] approaches. For most cases the present results agree with the previous work. For some transitions to the 2^+ state, the NMEs calculated in this paper are the smallest.

In most cases the branching ratios for the 2νECEC transitions to the ground state are very close to 1. For the $2\nu\beta^+$/EC decays to the ground state of ^{78}Kr, it is of interest to find that the 2νECEC (Br $\approx 61\%$) and $2\nu\beta^+$EC (Br $\approx 39\%$) transitions compete with each other. The Q value for this decay is 2.848 MeV and the phase space factors for $2\nu\beta^+$EC and 2νECEC are comparable. At present only the experimental results for the double-K capture of the ^{78}Kr nucleus are available [27]. For a better understanding of the $2\nu\beta^+$/EC decays of the ^{78}Kr nucleus, the half life of the $2\nu\beta^+$EC transition should also be measured.

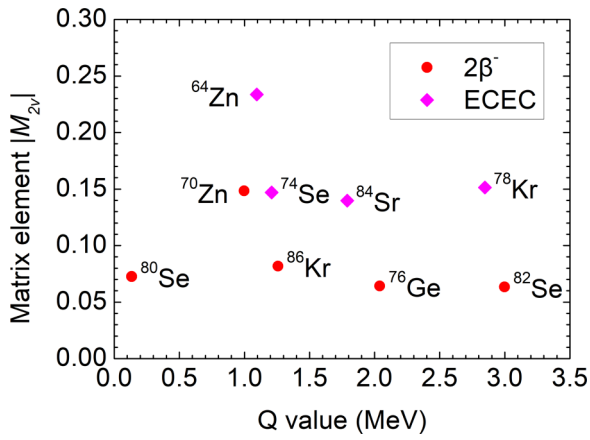

FIG. 3. The NME as a function of Q value for concerned nuclei. Triangles and diamonds represent the $2\nu 2\beta^-$ and 2νECEC types, respectively.

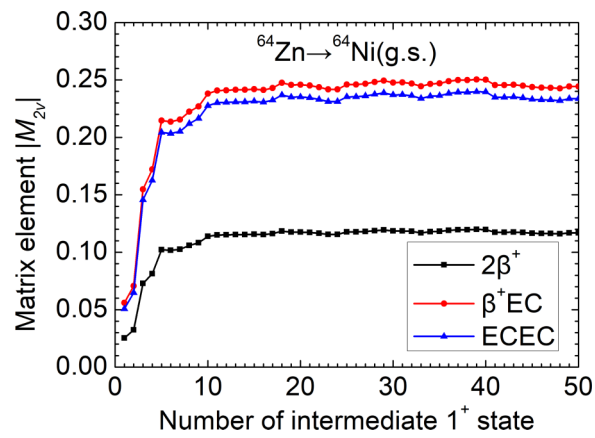

FIG. 4. The accumulations of the NMEs of ^{64}Zn decays to ground state. Decays for the $2\nu 2\beta^+$, $2\nu\beta^+$EC, and 2νECEC types are represented by the squares, circles, and triangles respectively. The SSDH, in this case, is not realized.

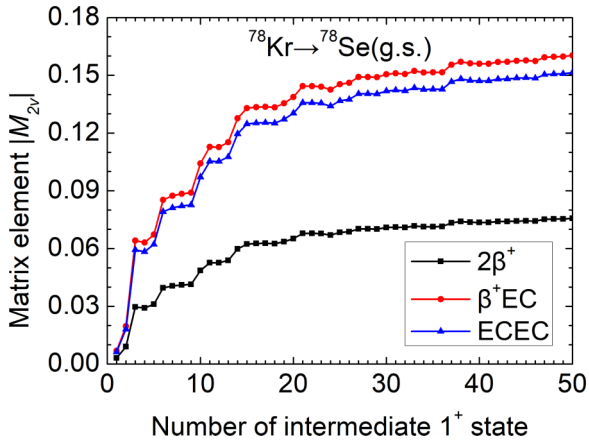

FIG. 5. The accumulations of the NMEs of ^{78}Kr decays to ground state. Decays for the $2\nu2\beta^+$, $2\nu\beta^+$EC, and 2νECEC types are represented by the squares, circles, and triangles respectively. The SSDH is not satisfied.

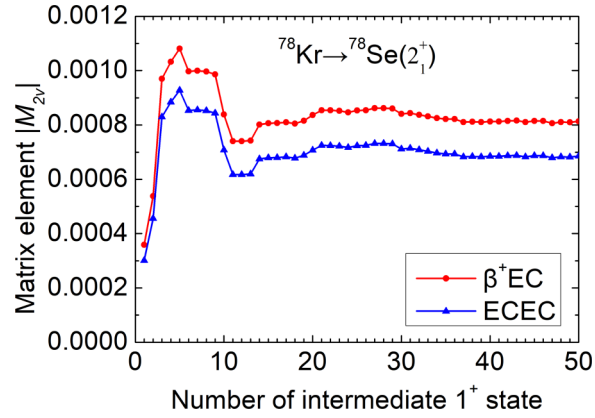

FIG. 7. The accumulations of NMEs of ^{78}Kr decays to the 2_1^+. Decays for the $2\nu\beta$EC and 2νECEC types are represented by the circles and triangles respectively. The SSDH, in this case, is not satisfied.

The NMEs play important roles in the $2\nu\beta\beta$ decay. Unlike the phase space factors which are well known, the NMEs depend on the structures of the nuclei which are of interest and difficult to calculate. In the $2\nu\beta\beta$ decays, transition to the ground state of the daughter nuclei dominates. The NMEs for these transitions are plotted as a function of the Q values in Fig. 3 where triangles and diamonds are for the $2\nu2\beta^-$ and 2νECEC types, respectively. All the data are from Tables II and III.

From Fig. 3 it is obvious that the NMEs do not depend on the Q value significantly. It is of interest to find that for most cases the NMEs for 2νECEC are systematically larger than that of $2\nu2\beta^-$. This phenomenon is not just a coincidence. Comparing Eqs. (4) and (8) one finds that the quantity $F_m^{2\beta^-}(0^+)$ is approximately half of the quantity $F_m^{\mathrm{ECEC}}(0^+)$ which leads to smaller NMEs for the $2\nu2\beta^-$.

Theoretically there exists the SSDH which suggests that the decay rate of the $2\nu2\beta$ is solely determined by virtual single-β transitions via the 1^+ ground state of the intermediate nucleus [34,35]. If the SSDH is confirmed then the corresponding NMEs could be determined from β decay measurements. Thus, it is of interest to analyze how the NMEs are accumulated. In the fpg shell the $2\nu2\beta$ decays of four nuclei (^{64}Zn, ^{70}Zn, ^{78}Kr, and ^{80}Se) are with intermediate nucleus whose ground state is 1^+. The accumulations of the NMEs for these nuclei are analyzed.

Accumulations of the NMEs for the $2\nu\beta^+$/EC decays of ^{64}Zn are depicted in Fig. 4. The running sums of the NMEs gain their final magnitude mainly from the first ten intermediate states. In this case, the SSDH is not satisfied. The nucleus ^{78}Kr can decay to the ground and excited states of the ^{78}Se nucleus. Accumulations of the NMEs are depicted in Figs. 5–7 for the $2\nu\beta^+$/EC decays of ^{78}Kr to the ground, 0_1^+, and 2_1^+ states of ^{78}Se, respectively. One can see from these figures that until after several intermediate states, the sums of the NMEs saturate to their final magnitude. Obviously, the SSDH is not realized for these cases. Accumulation of the $2\nu2\beta^-$ decays of the

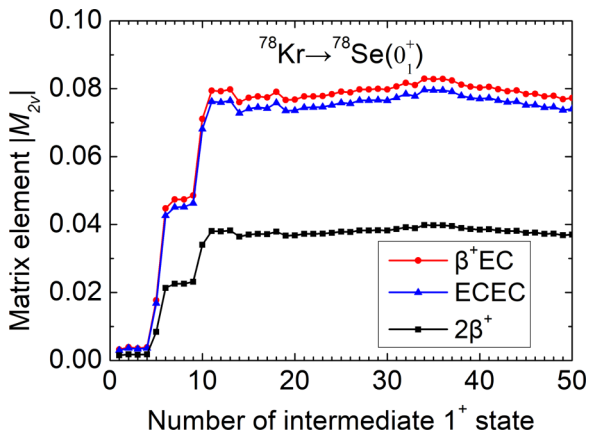

FIG. 6. The accumulations of the NMEs of ^{78}Kr decays to the 0_1^+. Decays for the $2\nu2\beta^+$, $2\nu\beta^+$EC, and 2νECEC types are represented by the squares, circles, and triangles respectively. The SSDH, in this case, is not realized.

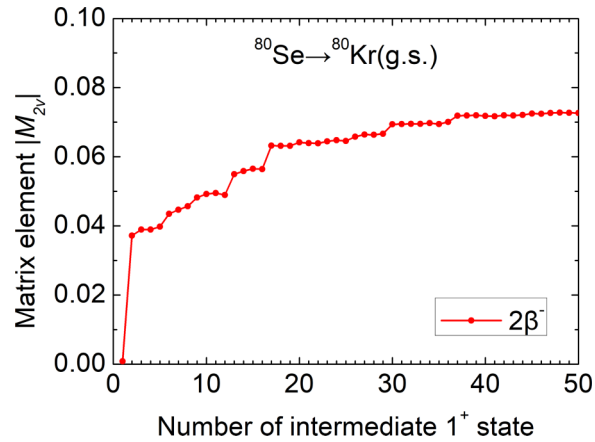

FIG. 8. The accumulation of the NME of ^{80}Se $2\nu2\beta^-$ decay to ground state. The main contribution to the NME comes from the second intermediate 1^+ state which the SSDH is not realized.

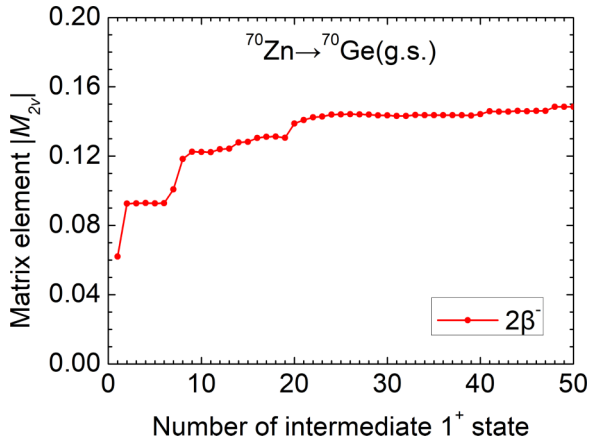

FIG. 9. The accumulation of the NME for the $2\nu 2\beta^-$ decay of ^{70}Zn to the ground state. The main contribution to the NME comes from the intermediate 1^+ ground state (about 42%).

^{80}Se and ^{70}Zn are depicted in Figs. 8 and 9, respectively. For the $2\nu 2\beta^-$ decay of ^{80}Se, the second intermediate 1^+ state contributes most to the NME and the SSDH is not satisfied. For the $2\nu 2\beta^-$ decay of ^{70}Zn, the sum of the NME gains 42% of its finial magnitude from the first intermediate state. Still, the SSDH is not realized.

By analyzing the accumulations of the NMEs, we find that the SSDH does not hold for all the transitions of the concerned nuclei. It should be noted that although the SSDH is not satisfied in these cases, there exist some intermediate 1^+ states whose contributions to the NME is significant. It is of interest to study whether for some cases the SSDH is approximately satisfied.

IV. SUMMARY AND CONCLUSIONS

In this paper the $2\nu\beta\beta$ decays for the fpg shell nuclei are studied systematically under the framework of nuclear shell model. The JUN45 effective interaction is used and all of the shell model calculations are carried out without any truncation. The axial-vector coupling constant $g_A = 1.27$ and the quenching factor $q = 0.73 \pm 0.07$ are adopted. Results for the calculated half lives, NMEs, phase space factors, and branching ratios are shown. Good agreements between theory and experiments are reached.

According to the calculations, the nuclei ^{86}Kr, ^{70}Zn, and ^{84}Sr are predicted to have relatively short half lives of 4.2×10^{22}, 1.4×10^{23}, and 1.9×10^{23} year respectively which seems attractive for future experimental probing. It is of interest to find that the 2νECEC (Br $\approx$ 61%) and $2\nu\beta^+$EC (Br $\approx$ 39%) modes compete with each other in the decay of ^{78}Kr. The half life of ^{78}Kr can be obtained precisely if both of the 2νECEC and $2\nu\beta^+$EC modes are measured.

Accumulations of the NMEs are analyzed. From the calculated results we find that the SSDH is not satisfied by all the concerned nuclei (^{64}Zn, ^{70}Zn, ^{78}Kr, and ^{80}Se) whose intermediate nuclei are of 1^+ ground state. Thus it may not be a very good approximation to use the SSDH in estimating the NMEs of the $2\nu\beta\beta$ decays for the fpg shell nuclei. In the future it would be interesting to investigate whether the SSDH is satisfied for some nuclei and this is an open problem for other nuclei.

ACKNOWLEDGMENTS

The authors are very grateful to Professor B. A. Brown, Michigan State University, for providing us with the computer program NUSHELLX. The authors also express their sincere thanks to Dr. M. Lyu for valuable discussions. This work was supported by the National Natural Science Foundation of China (Grants No. 11647086, No. 11647085, No. 11535004, No. 11375086, No. 11175085, and No. 11235001), by the National Major State Basic Research and Development of China (Grant No. 2016YFE0129300), by the Research Fund of Doctoral Point (RFDP), Grant No. 20100091110028, and by the Science and Technology Development Fund of Macao under Grant No. 068/2011/A.

[1] M. Goeppert-Mayer, Phys. Rev. **48**, 512 (1935).
[2] S. R. Elliott, A. A. Hahn, and M. K. Moe, Phys. Rev. Lett. **59**, 2020 (1987).
[3] R. Saakyan, Annu. Rev. Nucl. Part. Sci. **63**, 503 (2013).
[4] R. Arnold, C. Augier, J. Baker, A. Barabash, G. Broudin, V. Brudanin, A. J. Caffrey, E. Caurier, V. Egorov, K. Errahmane, A. I. Etienvre, J. L. Guyonnet, F. Hubert, P. Hubert, C. Jollet, S. Jullian, O. Kochetov, V. Kovalenko, S. Konovalov, D. Lalanne *et al.*, Phys. Rev. Lett. **95**, 182302 (2005).
[5] H. S. Miley, F. T. Avignone, R. L. Brodzinski, J. I. Collar, and J. H. Reeves, Phys. Rev. Lett. **65**, 3092 (1990).
[6] A. S. Barabash, F. T. Avignone, J. I. Collar, C. K. Guerard, R. J. Arthur, R. L. Brodzinski, H. S. Miley, J. H. Reeves, J. R. Meier, K. Ruddick, and V. I. Umatov, Phys. Lett. B **345**, 408 (1995).
[7] H. V. Thomas, R. A. D. Pattrick, S. A. Crowther, D. J. Blagburn, and J. D. Gilmour, Phys. Rev. C **78**, 054606 (2008).
[8] J. Argyriades *et al.* (NEMO Collaboration), Phys. Rev. C **80**, 032501 (2009).
[9] J. Suhonen and O. Civitarese, Phys. Rep. **300**, 123 (1998).
[10] J. Suhonen, Nucl. Phys. A **864**, 63 (2011).
[11] B. A. Brown, D. L. Fang, and M. Horoi, Phys. Rev. C **92**, 041301 (2015), and references therein.
[12] J. Toivanen and J. Suhonen, Phys. Rev. C **55**, 2314 (1997).
[13] S. Unlu, Chin. Phys. Lett. **31**, 042101 (2014).
[14] M. Aunola and J. Suhonen, Nucl. Phys. A **602**, 133 (1996).
[15] A. Shukla, R. Sahu, and V. K. B. Kota, Phys. Rev. C **80**, 057305 (2009).
[16] M. Horoi and B. A. Brown, Phys. Rev. Lett. **110**, 222502 (2013).
[17] R. Sahu and V. K. B. Kota, Int. J. Mod. Phys. E **20**, 1723 (2011).
[18] J. Barea, J. Kotila, and F. Iachello, Phys. Rev. C **91**, 034304 (2015).
[19] P. Pirinen and J. Suhonen, Phys. Rev. C **91**, 054309 (2015).

[20] Y. Ren and Z. Ren, Phys. Rev. C **89**, 064603 (2014).
[21] Y. Ren and Z. Ren, Nucl. Sci. Technol. **26**, S20510 (2015).
[22] A. S. Barabash, Phys. Rev. C **81**, 035501 (2010).
[23] M. Agostini *et al.* (GERDA Collaboration), J. Phys. G: Nucl. Part. Phys. **42**, 115201 (2015).
[24] J. Kotila and F. Iachello, Phys. Rev. C **87**, 024313 (2013).
[25] E. Aprile *et al.* (XENON Collaboration), Phys. Rev. C **95**, 024605 (2017).
[26] K. Abe *et al.* (XMASS Collaboration), Phys. Lett. B **759**, 64 (2016).
[27] Yu. M. Gavrilyuk, A. M. Gangapshev, V. V. Kazalov, V. V. Kuzminov, S. I. Panasenko, and S. S. Ratkevich, Phys. Rev. C **87**, 035501 (2013).
[28] J. Suhonen, Phys. Rev. C **86**, 024301 (2012).
[29] Y. Ren and Z. Ren, Sci. China Phys. Mech. Astron. **58**, 1 (2015).
[30] D. S. Delion and J. Suhonen, Phys. Rev. C **95**, 034330 (2017).
[31] A. Faessler, L. Gastaldo, and F. Šimkovic, Phys. Rev. C **95**, 045502 (2017).
[32] D. Štefánik, F. Šimkovic, and A. Faessler, Phys. Rev. C **91**, 064311 (2015).
[33] F. Šimkovic, V. Rodin, A. Faessler, and P. Vogel, Phys. Rev. C **87**, 045501 (2013).
[34] O. Civitarese and J. Suhonen, Phys. Rev. C **58**, 1535 (1998).
[35] O. Civitarese and J. Suhonen, Nucl. Phys. A **653**, 321 (1999).
[36] P. Domin, S. Kovalenko, F. Šimkovic, and S. V. Semenov, Nucl. Phys. A **753**, 337 (2005).
[37] F. Šimkovic, P. Domin, and S. V. Semenov, J. Phys. G: Nucl. Part. Phys. **27**, 2233 (2001).
[38] M. Doi and T. Kotani, Prog. Theor. Phys. **87**, 1207 (1992).
[39] Y. Iwata, N. Shimizu, T. Otsuka, Y. Utsuno, J. Menéndez, M. Honma, and T. Abe, Phys. Rev. Lett. **116**, 112502 (2016).
[40] A. Gando, Y. Gando, T. Hachiya, A. Hayashi, S. Hayashida, H. Ikeda, K. Inoue, K. Ishidoshiro, Y. Karino, M. Koga, S. Matsuda, T. Mitsui, K. Nakamura, S. Obara, T. Oura, H. Ozaki, I. Shimizu, Y. Shirahata, J. Shirai, A. Suzuki *et al.* (KamLAND-Zen Collaboration), Phys. Rev. Lett. **117**, 082503 (2016).
[41] F. T. Avignone, S. R. Elliott, and J. Engel, Rev. Mod. Phys. **80**, 481 (2008).
[42] M. Honma, T. Otsuka, T. Mizusaki, and M. Hjorth-Jensen, Phys. Rev. C **80**, 064323 (2009).
[43] B. A. Brown and W. D. M. Rae, Nucl. Data Sheets **120**, 115 (2014).
[44] G. Martínez-Pinedo, A. Poves, E. Caurier, and A. P. Zuker, Phys. Rev. C **53**, R2602 (1996).
[45] E. J. Bai and J. D. Huo, Nucl. Data Sheets **92**, 147 (2001).
[46] B. Singh, Nucl. Data Sheets **108**, 197 (2007).
[47] E. Browne and J. K. Tuli, Nucl. Data Sheets **111**, 2425 (2010).
[48] E. Browne and J. K. Tuli, Nucl. Data Sheets **111**, 1093 (2010).
[49] J. D. Huo, X. L. Huang, and J. K. Tuli, Nucl. Data Sheets **106**, 159 (2005).
[50] E. A. McCutChan, Nucl. Data Sheets **113**, 1735 (2012).
[51] J. K. Tuli, Nucl. Data Sheets **103**, 389 (2004).
[52] A. R. Farhan and B. Singh, Nucl. Data Sheets **110**, 1917 (2009).
[53] B. Singh, Nucl. Data Sheets **105**, 223 (2005).
[54] Q. Zhi, E. Caurier, J. J. Cuenca-García, K. Langanke, G. Martínez-Pinedo, and K. Sieja, Phys. Rev. C **87**, 025803 (2013).
[55] H. Li and Z. Ren, J. Phys. G: Nucl. Part. Phys. **41**, 105102 (2014).
[56] E. Caurier, F. Nowacki, A. Poves, and J. Retamosa, Phys. Rev. Lett. **77**, 1954 (1996).
[57] P. Belli, R. Bernabei, F. Cappella, R. Cerulli, F. A. Danevich, S. d'Angelo, A. Incicchitti, V. V. Kobychev, D. V. Poda, and V. I. Tretyak, J. Phys. G: Nucl. Part. Phys. **38**, 115107 (2011).
[58] G. Audi, F. G. Kondev, M. Wang, W. J. Huang, and S. Naimi, Chin. Phys. C **41**, 030001 (2017).
[59] M. Agostini *et al.* (GERDA Collaboration), J. Phys. G: Nucl. Part. Phys. **40**, 035110 (2013).
[60] J. W. Beeman, F. Bellini, P. Benetti, L. Cardani, N. Casali, D. Chiesa, M. Clemenza, I. Dafinei, S. Di Domizio, F. Ferroni *et al.*, Eur. Phys. J. C **75**, 591 (2015).
[61] B. Lehnert, T. Wester, D. Degering, D. Sommer, L. Wagner, and K. Zuber, J. Phys. G: Nucl. Part. Phys. **43**, 085201 (2016).
[62] G. Audi and A. H. Wapstra, Nucl. Phys. A **595**, 409 (1995).